

## Research Article

# Stratifin-mediated activation of AKT signaling and therapeutic targetability in hepatocellular carcinoma progression

Rong Hua<sup>a</sup>, Kaitao Zhao<sup>a</sup>, Zaichao Xu<sup>a</sup>, Yingcheng Zheng<sup>a</sup>, Chuanjian Wu<sup>a</sup>, Lu Zhang<sup>a</sup>, Yan Teng<sup>a</sup>, Jingjing Wang<sup>a</sup>, Mengfei Wang<sup>a</sup>, Jiayu Hu<sup>a</sup>, Lang Chen<sup>b</sup>, Detian Yuan<sup>c</sup>, Wei Dong<sup>d,e,f,g,\*\*</sup>, Xiaoming Cheng<sup>a,h,i,j,\*\*\*</sup>, Yuchen Xia<sup>a,j,k,\*</sup>

<sup>a</sup> State Key Laboratory of Virology and Hubei Province Key Laboratory of Allergy and Immunology, Institute of Medical Virology, TaiKang Center for Life and Medical Sciences, TaiKang Medical School, Wuhan University, Wuhan, China

<sup>b</sup> Department of Immunology, TaiKang Medical School, Wuhan University, Wuhan, China

<sup>c</sup> Department of Biochemistry and Molecular Biology, School of Basic Medical Sciences, Cheeloo College of Medicine, Shandong University, Jinan, China

<sup>d</sup> Hepatic Surgery Center, Tongji Hospital, Tongji Medical College, Huazhong University of Science and Technology, Wuhan, Hubei, China

<sup>e</sup> Hubei Key Laboratory of Hepato-Pancreato-Biliary Diseases, Wuhan, Hubei, China

<sup>f</sup> Hubei Province for the Clinical Medicine Research Center of Hepatic Surgery, Wuhan, Hubei, China

<sup>g</sup> Key Laboratory of Organ Transplantation, Ministry of Education, NHC Key Laboratory of Organ Transplantation, Chinese Academy of Medical Sciences, Wuhan, Hubei, China

<sup>h</sup> Wuhan University Center for Pathology and Molecular Diagnostics, Zhongnan Hospital of Wuhan University, Wuhan, China

<sup>i</sup> Hubei Clinical Center and Key Laboratory of Intestinal and Colorectal Diseases, Wuhan, China

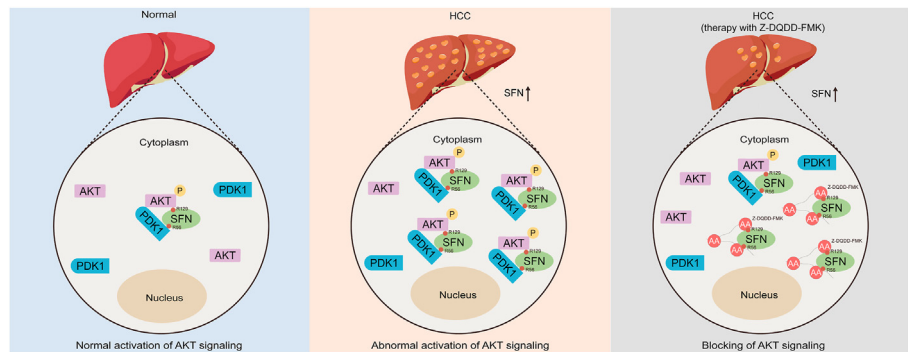
<sup>j</sup> Hubei Jiangxia Laboratory, Wuhan, China

<sup>k</sup> Pingyuan Laboratory, Henan, China

## HIGHLIGHTS

- SFN activates AKT signaling by fostering the interaction between PDK1 and AKT1 in HCC.
- The Arg-56 and Arg-129 residues in SFN are essential for bridging PDK1 and AKT1.
- Z-DQDD-FMK, a peptide inhibitor blocking SFN, significantly inhibits HCC progression.

## GRAPHICAL ABSTRACT



## ARTICLE INFO

**Keywords:**  
Hepatocellular carcinoma  
SFN

## ABSTRACT

Hepatocellular carcinoma (HCC) is the third leading cause of cancer-related deaths worldwide and presents a significant threat to human health. Despite its prevalence, the underlying regulatory mechanisms of HCC remain unclear. In this study, we integrated RNA-seq datasets, proteome dataset and survival analysis and unveiled Stratifin (SFN) as a potential prognostic biomarker for HCC. SFN knockdown inhibited HCC progression in cell

\* Corresponding author. Institute of Medical Virology, TaiKang Medical School, Wuhan University, Wuhan, 430071, China.

\*\* Corresponding author. Hepatic Surgery Center, Tongji Hospital, Tongji Medical College, Huazhong University of Science and Technology, Wuhan, Hubei, China.

\*\*\* Corresponding author. Department of Pathophysiology, TaiKang Medical School, Wuhan University, Wuhan, China.

E-mail addresses: [wei.dong@tjh.tjmu.edu.cn](mailto:wei.dong@tjh.tjmu.edu.cn) (W. Dong), [xiaoming.cheng@whu.edu.cn](mailto:xiaoming.cheng@whu.edu.cn) (X. Cheng), [yuchenxia@whu.edu.cn](mailto:yuchenxia@whu.edu.cn) (Y. Xia).

<https://doi.org/10.1016/j.cellin.2024.100178>

Received 10 April 2024; Received in revised form 14 May 2024; Accepted 15 May 2024

2772-8927/© 2024 The Author(s). Published by Elsevier B.V. on behalf of Wuhan University. This is an open access article under the CC BY-NC-ND license (<http://creativecommons.org/licenses/by-nc-nd/4.0/>).

cultures and mouse models. Conversely, ectopic expression of Sfn in primary mouse HCC model accelerated HCC progression. Mechanistically, SFN acted as an adaptor protein, activating AKT1 signaling by fostering the interaction between PDK1 and AKT1, with the R56 and R129 sites on SFN proving to be crucial for this binding. In the syngeneic implantation model, the R56A/R129A mutant of SFN inhibited Akt signaling activation and impeded HCC growth. Additionally, peptide inhibitors designed based on the binding motif of AKT1 to SFN significantly inhibited HCC progression. In summary, our findings establish that SFN promotes HCC progression by activating AKT signaling through the R56 and R129 binding sites. This discovery opens new avenues for a promising therapeutic strategy for the treatment of HCC.

## 1. Introduction

Primary liver cancer is the sixth most commonly diagnosed cancer and the third leading cause of cancer-related death worldwide, posing a serious threat to human health (Sung et al., 2021). Primary liver cancer is mainly composed of hepatocellular carcinoma (HCC) (accounting for 75%–85%) and intrahepatic cholangiocarcinoma (accounting for 10%–15%). The main risk factors for HCC are hepatitis virus infection (Plummer et al., 2016), aflatoxin exposure, alcohol intake, being overweight, type 2 diabetes, and smoking (Llovet et al., 2021). The prevention and treatment of HCC are crucial for public health.

The treatment of HCC mainly includes surgical resection (Marasco et al., 2019), liver transplantation, radiotherapy, chemotherapy (Llovet et al., 2002), systemic treatment with inhibitors, such as sorafenib (Llovet et al., 2022) and lenvatinib (Kudo et al., 2018), and immunotherapy (Liu et al., 2024). Owing to the lack of suitable HCC biomarkers, most patients are already in advanced stages when diagnosed with HCC. Although surgical excision improves the 5-year overall survival, the tumor recurrence is the high incidence (Vogel et al., 2022). Radiotherapy has anti-tumor activity, but survival benefit has not been proven. Systemic chemotherapy has frequent toxic effects without survival benefit (Forner et al., 2012). Theoretically, liver transplantation is an optimal therapeutic option, as it significantly enhances survival rates and reduces HCC recurrence. However, the shortage of donors and strict indications for advanced liver cancer remain the primary limitation of liver transplantation (Sapisochin & Bruix, 2017). Sorafenib and lenvatinib are kinase inhibitors, have anti-proliferative and anti-angiogenic effects, and have been approved for the systemic treatment of HCC. However, a single-drug treatment can promote drug tolerance in patients with HCC (Lencioni et al., 2014). Immunotherapy represents a monumental breakthrough in cancer treatment. For example, combination therapy with PD-L1 blockade and CTLA-4 blockade enhances the overall response rate of HCC patients. However, there is a need to develop more effective and less toxic treatment strategies (Liu et al., 2024). To innovate and advance HCC treatment strategies, it is crucial to uncover the underlying regulatory mechanisms.

The development of hepatocellular carcinoma involves complex, multistep processes (Forner et al., 2018). Previous studies have highlighted the aberrant activation of several signaling pathways in HCC, including the RAS/MAPK signaling pathway (Schulze et al., 2016) and PI3K/AKT pathway (Pellegrino et al., 2014). The Ras-Raf-MEK-ERK signaling pathway, commonly known as the RAS/MAPK pathway, is a classical kinase cascade (Neuzillet et al., 2014). Phosphatidylinositol-3 kinases (PI3Ks) constitute a lipid kinase family that catalyzes phosphatidylinositol-4,5-bisphosphate (PI-4,5-P2) to generate the second messenger phosphatidylinositol-3,4,5-trisphosphate (PI-3,4,5-P3), which then activate AKT (Mayer & Arteaga, 2016). AKT activation plays an important role in cell proliferation, migration, survival, glucose metabolism, and protein synthesis (Hoxhaj & Manning, 2020). Aberrant AKT activation has been observed in various cancer types and sustained activation can induce primary HCC in mice (Liu et al., 2021). Although some mechanisms controlling HCC have been identified, treatment options remain limited. Identifying novel genes that regulate HCC is crucial for identifying new therapeutic targets and strategies for combating this disease.

In this study, we identified Stratifin (SFN) as a potential regulator of HCC progression that facilitates the interaction between PDK1 and AKT1. A novel peptide inhibitor designed based on the binding motif of AKT1 significantly inhibited HCC progression. Our study not only elucidates the underlying mechanism of SFN in regulating HCC progression but also provides a promising therapeutic strategy that could have substantial clinical benefits.

## 2. Results

### 2.1. SFN is highly expressed in HCC

To discover novel HCC therapeutic targets, we conducted a comparative analysis of clinical HCC RNA-seq datasets GSE124535 (Jiang et al., 2019) and GSE14520 (Roessler et al., 2010) (Fig. 1A) and identified 28 upregulated genes (Supplementary Fig. S1A). Of the 28 up-regulated genes, adenylyl cyclase-associated protein 2 (CAP2), denticleless protein homolog (DTL), SFN and sulfotransferase family 1C member 2 (SULT1C2) have not been demonstrated to regulate the progression of HCC. We then evaluated the protein levels of these genes in paired non-tumor and tumor HCC samples from the HCC proteome dataset. While the protein levels of CAP2, SFN, and SULT1C2 were upregulated in the tumor samples, the DTL protein level remained unchanged (Fig. 1B). Survival analysis using GEPIA showed that high levels of SFN and DTL, but not CAP2 and SULT1C2, were associated with poor HCC prognosis (Fig. 1C). Therefore, the SFN was chosen for further studies. Consistently, elevation of SFN mRNA and protein levels was confirmed in paired HCC patient samples (Fig. 1D and E). Taken together, high levels of SFN expression in HCC tissues are positively correlated with poor prognosis, suggesting that SFN promotes HCC progression.

### 2.2. SFN affects the proliferation and migration of HCC cells

To investigate the role of SFN in HCC cell lines, we conducted SFN knockdown in the HepG2, Huh7, and Li-7 cell lines. The verification of SFN knockdown was confirmed at both mRNA and protein levels (Fig. 2A and B, Supplementary Fig. S2A). Interestingly, SFN knockdown significantly inhibited the proliferation of HCC cells (Fig. 2C and D, Supplementary Figs. S2B and C), and migration (Fig. 2E and Supplementary Fig. S2D). Notably, the upregulation of E-cadherin, a key regulator of cell-cell adhesion (Na et al., 2020), was observed in SFN-knockdown HCC cells (Fig. 2F), suggesting that SFN plays a role in promoting HCC cell migration. In conclusion, SFN inhibition significantly influences the proliferation and migration of HCC cells.

### 2.3. SFN promotes HCC development *in vivo*

To assess the effect of SFN on tumorigenicity *in vivo*, we initiated SFN depletion through lentiviral transduction of shRNA in Hepa1-6 cells, a mouse HCC cell line with high expression of SFN (Fig. 3A, Supplementary Figs. S3A and B). As expected, SFN depletion inhibited HCC cell proliferation (Fig. 3B and C) *in vitro*. Notably, three weeks after subcutaneous inoculation of Hepa1-6 cells into C57BL/6 mice (Fig. 3D), we observed a substantial reduction in tumor size in the Sfn low expression group (Fig. 3E and F). These findings underscore the indispensable role of SFN

in HCC tumor progression in an orthotopic xenograft model.

Recognizing the environmental nuances influencing HCC cells *in vivo*, the mouse primary HCC model has emerged as a closer representation of clinical HCC incidence and progression. The mouse primary HCC model was established by hydrodynamic tail vein gene delivery of the *c-Myc* transposon system and a CRISPR-Cas9 vector targeting *Tp53* (Tang et al., 2022) and further ectopic expression of the *Sfn* gene via the AAV vector through the tail vein (Fig. 4A). At 37 days post-injection, ectopic expression of SFN accelerated mouse primary HCC progression *in vivo* (Fig. 4B). Consistently, the largest tumor size (Fig. 4C) and number (Fig. 4D) were increased in *Sfn* ectopically expressed mouse livers. SFN expression was validated using immunoblotting (Fig. 4E). Similar to paired human samples, SFN protein levels were higher in tumor tissues than in adjacent tissues (Supplementary Fig. S3C). To delve deeper into the influence of SFN on HCC tumorigenesis, we performed hydrodynamic gene delivery of SFN via the tail vein (Fig. 4F). This approach led to the identification of numerous liver nodules in mice ectopically expressing *Sfn* (Fig. 4G). Histological examination by H&E (Fig. 4H) and Ki-67 (Fig. 4I) staining revealed the presence of primary HCC cells in these mice. Taken together, SFN merges as a potential oncogene for HCC and plays an important role in HCC tumorigenesis.

#### 2.4. SFN activates AKT signaling

To elucidate the mechanism underlying the role of SFN in HCC progression, we performed SFN immunoprecipitation mass spectrometry in Huh7 cells. SFN interaction partners were enriched in both the MAPK and PI3K-AKT signaling pathways (Fig. 5A). However, SFN knockdown did not significantly affect the expression of MAPK signaling pathway-related genes (Fig. 5B and C). In contrast, regarding the PI3K-AKT signaling pathway, SFN knockdown had no effect on the mRNA

expression levels of AKT upstream genes (Fig. 5D) or the activation of AKT upstream signals but exhibited a notable inhibition of AKT and GSK3 $\beta$  phosphorylation (Fig. 5E). Furthermore, ectopic expression of SFN activated AKT signaling (Fig. 5F). Collectively, these findings suggest that SFN promotes HCC progression by specifically activating the AKT signaling pathway.

#### 2.5. SFN promotes the interaction between PDK1 and AKT1

As an adaptor protein, SFN binds a large number of proteins to regulate signaling pathways (Kaplan et al., 2017). Whether SFN activates the AKT signaling pathway by interacting directly with AKT warrants further exploration. Our investigation revealed that SFN could interact with AKT1, as demonstrated by co-immunoprecipitation (Fig. 6A) and GST pull-down assays (Fig. 6B, Supplementary Figs. S4A and S4B), indicating direct interaction between SFN and AKT1. To dissect the specific region of interaction between AKT1 and SFN, we constructed truncated AKT1 variants. Interestingly, deletion of the AKT1 PH domain and protein kinase domain had no effect on its interaction with SFN (Fig. 6C), whereas deletion of the AKT1 AGC-kinase domain significantly inhibited its interaction with SFN (Fig. 6D). Further examination of the C-terminally truncated mutants revealed that AKT1 interacted with SFN through its 445–462 amino acids (Fig. 6E).

Previous studies have identified SFN R56 and R129 residues as crucial for the interaction with phosphoserine or phosphothreonine in interacting proteins (Shiba-Ishii et al., 2019). To verify the role of R56 and R129 in the interaction between SFN and AKT1, we constructed the SFN R56A and R129A mutants. As detected, the SFN R129A rather than R59A mutation weakened the interaction with AKT1 (Fig. 6F), suggesting that SFN R129 participates in the interaction with AKT1. Intriguingly, mutations in the serine and threonine residues within the AGC-kinase

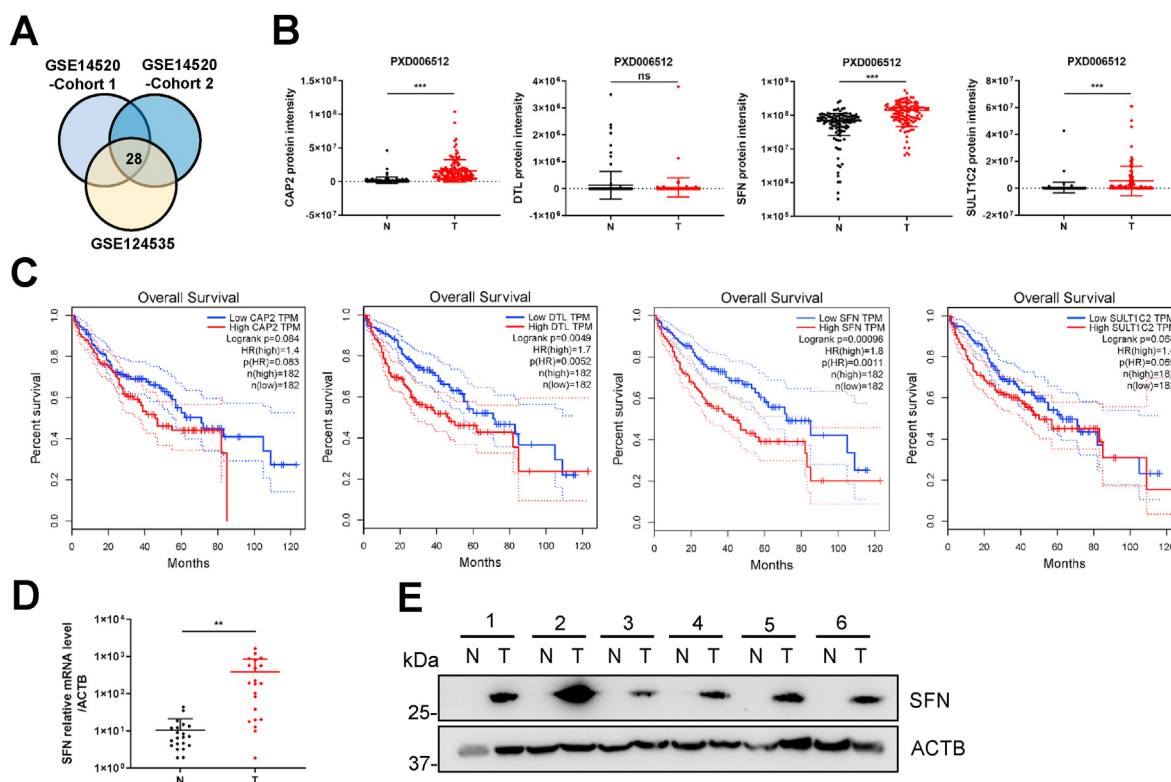


**Fig. 1.** High expression levels of SFN in HCC are positively correlated to the poor prognosis of cancer patients.

(A) Venn diagram of screening for potential genes involved in HCC progression. (B) Comparisons of CAP2, DTL, SFN and SULT1C2 protein level between paired non-tumor and tumor HCC samples ( $n = 124$ ) from PXD006512. (C) Overall survival analysis for CAP2, DTL, SFN and SULT1C2 expression levels by GEPIA. (D) Comparisons of SFN mRNA level between paired non-tumor and tumor HCC samples ( $n = 21$ ) surgically resected from HCC patients. (E) Immunoblot analysis of SFN in paired non-tumor and tumor HCC samples ( $n = 6$ ) surgically resected from HCC patients.

domain of AKT1 had no effect on its interaction with SFN, indicating that the interaction between SFN and AKT1 was independent of serine or threonine (Fig. 6D, Supplementary Fig. S4C).

Previous studies have implicated the protein kinases PDK1 and TBK1 in activating AKT1 through direct interaction (Cooper et al., 2017; Jiang et al., 2022). We hypothesized that SFN promotes AKT1 activation by enhancing the interactions between AKT1 and TBK1 or PDK1. Ectopic expression of SFN facilitated the interaction between AKT1 and PDK1 (Fig. 6G) but not TBK1 (Fig. 6H). SFN knockdown also impaired the interaction between AKT1 and PDK1 (Fig. 6I). Further analysis of SFN mutants revealed that SFN interacting with PDK1 relies on its R56 and R129 residues (Fig. 6J). Taken together, our findings indicate that SFN promotes the interaction between PDK1 and AKT1, thereby shedding light on its role in AKT1 activation.

## 2.6. SFN R56 and R129 are important for AKT activation and HCC progression *in vivo*

Although it has been demonstrated that SFN R56 and R129 are involved in interacting with AKT1 and PDK1, their specific roles in regulating HCC progression remain unknown. To determine the role of SFN R56 and R129 in HCC, we generated R56 and R129 mutants in mouse hepatoma H22 cells (Fig. 7A). Notably, ectopic expression of SFN promoted H22 cell proliferation, whereas SFN mutants had no discernible effect on the cells (Fig. 7B).

To further validate the influence of SFN mutations on cell tumorigenicity, we subcutaneously implanted H22 cells into mice (Fig. 7C). By 21 days post implantation, ectopic expression of SFN accelerated mouse HCC cell tumorigenicity *in vivo*. In contrast, the ectopic expression of the Sfn mutant had no effect on mouse HCC cells (Fig. 7D). Consistently, the Sfn mutant weakened the promotion of Sfn on tumor size (Fig. 7E), tumor

weight (Fig. 7F), and tumor growth (Fig. 7G). Moreover, SFN activated AKT in mouse HCC cells, whereas the SFN mutant failed to activate AKT (Fig. 7H). In summary, our findings indicate that SFN R56 and R129 play crucial roles in regulating AKT activation and HCC progression through their participation in the interaction between AKT1 and PDK1. This underscores the potential of SFN R56 and R129 as therapeutic targets for HCC treatment.

## 2.7. PDQDDS inhibits HCC growth by competitive binding SFN with AKT1

In our pursuit of impeding the function of SFN in HCC, we aimed to develop potential SFN inhibitors. A novel strategy involves designing polypeptide drugs from an acidic amino acid-rich motif, which competitively binds to SFN and AKT1, thereby inhibiting the aberrant activation of AKT1 for HCC treatment. Our findings from AKT1 deletion mutants point towards the crucial role of the 445–462 amino acid motif in SFN binding. Further exploration through molecular docking revealed that the PDQDDS motif of AKT1 docked with R56 and R129 of SFN (Fig. 8A).

To validate the functional impact of the PDQDDS, we constructed P2A-linked expression vectors for PDQDDS and GFP (Supplementary Fig. S5A). As expected, PDQDDS expression inhibited HCC cell proliferation (Fig. 8B and C, Supplementary Figs. S5B and C), and migration (Fig. 8D, Supplementary Fig. S5D). To further validate the influence of PDQDDS on tumorigenicity, we subcutaneously implanted H22-PDQDDS cells into mice (Fig. 8E). By 16 days post-implantation, overexpression of PDQDDS inhibited mouse HCC cell tumorigenicity *in vivo* (Fig. 8F). Consistently, PDQDDS inhibited tumor size (Fig. 8G) and weight (Fig. 8H). PDQDDS expression was validated using immunoblotting (Supplementary Fig. S5E). Therefore, drugs designed based on the PDQDDS motif have the potential to treat HCC.

Considering that R56 and R129 of SFN are more likely to bind with

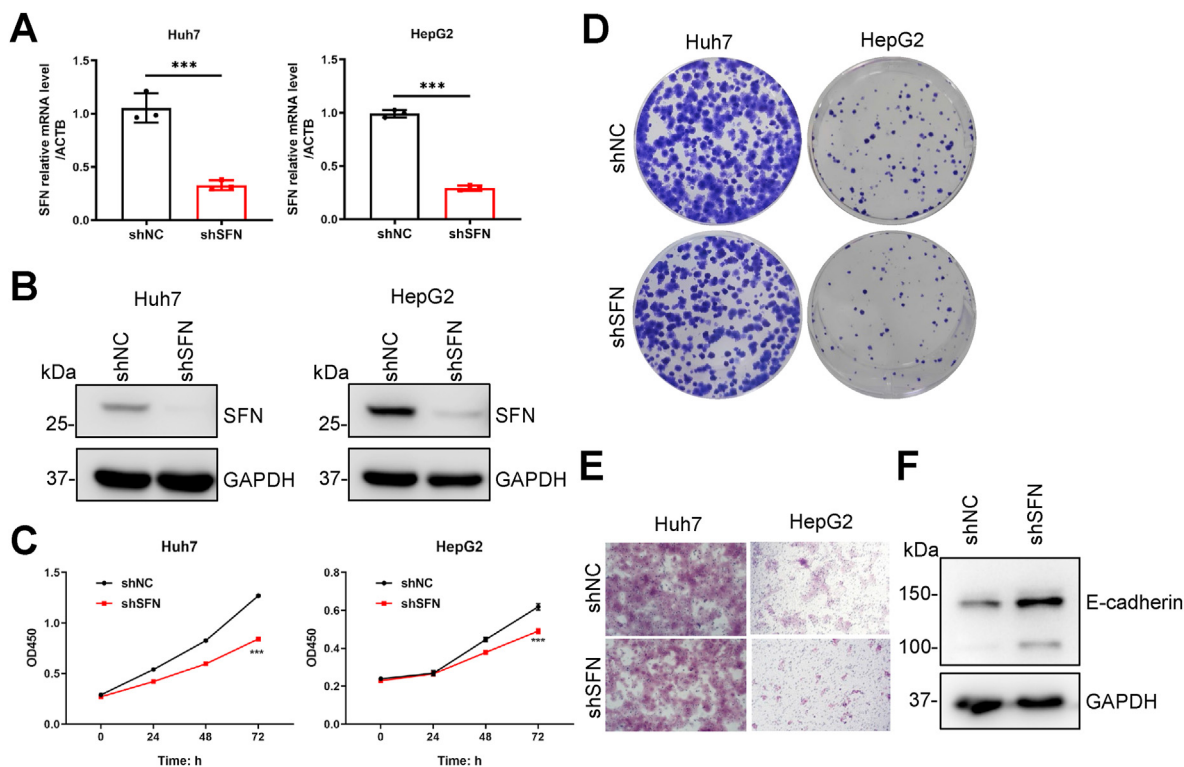


**Fig. 2. Inhibition of SFN affects the proliferation and migration of HCC cells.** Huh7 and HepG2 cells were infected with lentivirus encoding shRNA targeting SFN or shNC (negative control) for at least four days.

(A) SFN knockdown was validated by measuring the mRNA levels of SFN in Huh7 and HepG2 cell lines. (B) SFN knockdown was validated by measuring the protein levels of SFN in Huh7 and HepG2 cell lines. (C) Cell proliferation was measured using CCK8 in SFN-KD Huh7 and HepG2 cell lines. (D) Cell proliferation was measured by colony formation assay in SFN KD Huh7 and HepG2 cells. (E) Cell migration was measured by transwell assay in SFN KD Huh7 and HepG2 cell lines. (F) E-cadherin protein levels were assayed in SFN KD HepG2 cells.

acidic amino acids, a peptide drug was designed based on DQDD. To enhance the stability of the peptide drug, a benzyloxycarbonyl group (Z) was linked to the N-terminus of DQDD. As expected, Z-DQDD treatment inhibited HCC cell proliferation (Supplementary Figs. S6A and B) and the interaction between SFN, PDK1, and AKT1 (Supplementary Fig. S6C). Additionally, a fluoromethylketone group (FMK) was linked to the C-terminus of Z-DQDD to improve membrane permeability. As expected, Z-DQDD-FMK inhibited the proliferation of HCC cells (Fig. 8I and J) and the interaction between PDK1 and AKT1 (Fig. 8K). To validate the efficacy of Z-DQDD-FMK *in vivo*, we subcutaneously implanted H22 cells into mice and intratumorally administered Z-DQDD-FMK (Fig. 8L). By 21 days post implantation, Z-DQDD-FMK inhibited mouse HCC cell tumorigenicity *in vivo* (Fig. 8M). Consistently, Z-DQDD-FMK inhibited tumor growth (Fig. 8N) and tumor weight (Fig. 8O).

Taken together, expression of PDQDDs inhibited HCC growth by blocking the interaction between SFN and AKT1, design peptide according to DQDD is a promising therapeutic strategy for HCC.

### 3. Discussion

In the present study, we demonstrated that SFN, an adaptor protein involved in multiple signaling pathways, plays a role in promoting HCC tumorigenesis. SFN is aberrantly upregulated and correlates with poor prognosis in HCC. SFN knockdown significantly impaired HCC progression both *in vitro* and *in vivo*. Conversely, ectopic expression of Sfn in hydrodynamic tail vein gene delivery of the c-Myc transposon system and a CRISPR-Cas9 vector targeting Tp53 induced mouse HCC model accelerated HCC progression. Mechanistically, IP-mass analysis followed by validation suggests that SFN regulates AKT activation. As an adaptor protein, SFN promotes the interaction between PDK1 and AKT1 at the R56 and R129 sites. Additionally, peptide inhibitors designed based on the binding motif of AKT1 to SFN significantly inhibited HCC progression, which provides a promising therapeutic strategy for HCC.

SFN belongs to the 14-3-3 protein family and serves as an adapter protein (Chen et al., 2018). Through binding to various substrate proteins, SFN mediates diverse signaling pathways, including cell cycle

regulation, apoptosis, cell proliferation, metabolic regulation, and protein trafficking (Pair & Yacoubian, 2021). The role of SFN varies among different cancer types. For instance, in colorectal cancer, the expression of SFN is regulated by the tumor suppressor gene P53, leading to G2 arrest and inhibition of tumor progression (Hermeking et al., 1997). In breast cancer, SFN stabilizes P53 by regulating the self-ubiquitination and degradation of MDM2, thereby suppressing tumor growth (Yang et al., 2003). However, recent studies have reported elevated SFN expression in specific cancers. In lung cancer, SFN induces autophagy through nucleation of the Vps34-BECN1-TRAF6 complex, thus promoting tumor progression (Kim et al., 2022). In lung adenocarcinoma, SFN promotes RTK stability by interacting with USP8 to accelerate tumor growth (Kim et al., 2018). High expression of SFN is reported to be associated with poor prognosis of HCC (Yang et al., 2020; Zhao et al., 2023), the molecular mechanism by which SFN regulates HCC remains unclear. This study revealed that SFN promotes HCC progression by activating the AKT signaling pathway, contributing to a more comprehensive understanding of the role of SFN in HCC.

Given that HBV is the primary cause of HCC (Zhao et al., 2020), understanding SFN's potential role in HCC becomes crucial, particularly in distinguishing its effects in individuals with and without HBV infection. In our investigation, we observed elevated SFN expression in clinical samples of HBV-related HCC (Fig. 1D and E), suggesting a potential link between SFN and the progression of HCC in the context of HBV infection. Moreover, our *in vitro* (Fig. 2) and *in vivo* (Figs. 3 and 4) experiments conducted in HCC models devoid of HBV infection revealed a notable role for SFN in driving HCC progression. Consequently, our findings preliminarily suggest SFN's involvement in promoting HCC advancement, irrespective of HBV infection status. Nonetheless, further experimental evidence is warranted to solidify this conclusion.

SFN is located in the cytoplasm, but can also be secreted into the extracellular space, potentially offering a new biomarker for disease diagnosis. Diffuse alveolar damage is associated with a poor prognosis in patients with drug-induced interstitial lung disease, and serum SFN is a promising diagnostic biomarker for this condition (Arakawa et al., 2022). Clinical sample analysis demonstrated a positive correlation between

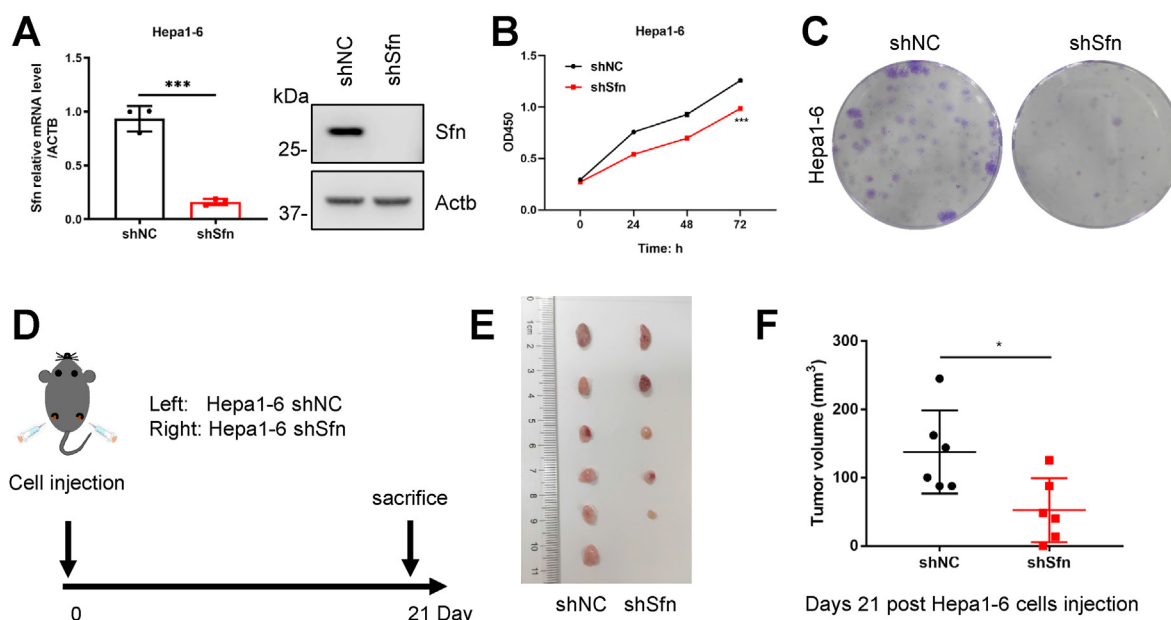


**Fig. 3. Decreasing SFN expression inhibited HCC development.**

(A–C) Hepa1-6 cells were infected with lentivirus encoding shRNA targeting Sfn or shNC (negative control) for 4 days. Sfn knockdown of mRNA level (left) and protein level (right) was validated (A). Cell proliferation was measured by CCK8 in Sfn KD Hepa1-6 cell line (B). Cell proliferation was measured by colony formation assay in Sfn KD Hepa1-6 cell line (C). (D) Schematic for implantation assay. Mice were subcutaneously injected with  $1.3 \times 10^6$  Hepa1-6 shSfn cells and Hepa1-6 shNC cells to generate a tumor model. Mice were sacrificed days 21 post Hepa1-6 cells injection. (E) Photographs of tumors 21 days post injection of control and Sfn KD Hepa1-6 cells implantation.  $n = 6$ . (F) Quantification of tumor volume from control and Sfn KD Hepa1-6 cells implantation 21 days post injection.  $n = 6$ .

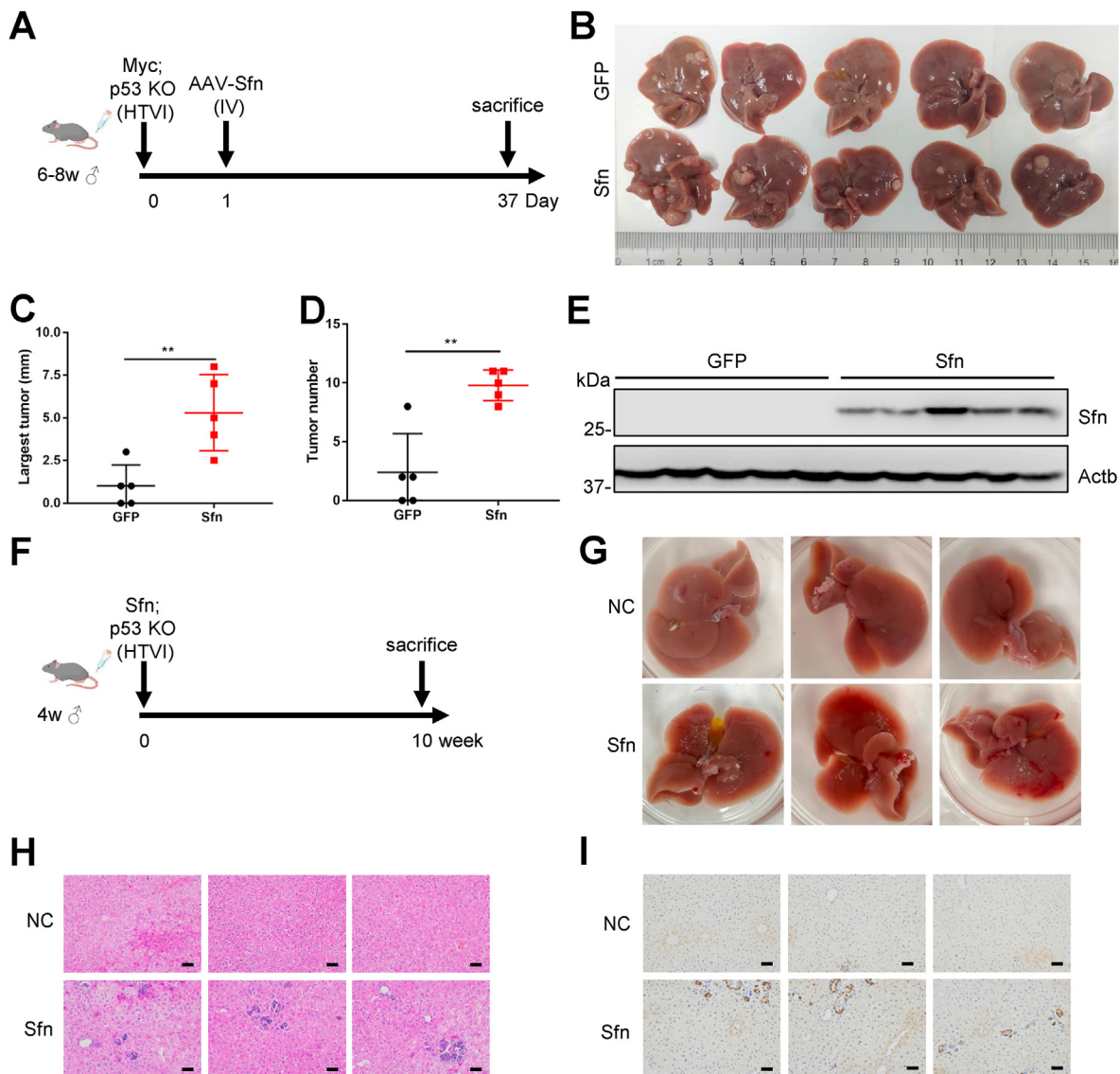


**Fig. 4. High SFN expression drives HCC tumorigenesis.**

(A) Schematic for inducing mouse liver cancer by hydrodynamic tail vein gene delivery of the c-Myc transposon system and a CRISPR-Cas9 vector targeting Tp53, infected with AAV-Sfn ( $n = 5$ ) or AAV-GFP ( $n = 5$ ) one day after hydrodynamic tail vein injection. (B) Shown are liver images of GFP and Sfn mice. (C) The largest tumor size of GFP and Sfn mice. (D) The tumor number of GFP and Sfn mice. (E) Immunoblot analysis of Sfn of GFP and Sfn mice liver. (F) Schematic for hydrodynamic tail vein gene delivery of the Sfn ( $n = 3$ ) or empty vector control (NC,  $n = 3$ ) transposon system and a CRISPR-Cas9 vector targeting Tp53, mice were sacrificed 10 weeks after injection. (G) Shown are liver images of NC and Sfn overexpression mice. (H) H&E staining of NC and Sfn overexpression mouse liver tissues. Scale bars, 50  $\mu\text{m}$ . (I) Ki-67 staining of NC and Sfn overexpression mouse liver tissues. Scale bars, 50  $\mu\text{m}$ .

serum SFN levels and the metastasis and progression of breast cancer, indicating that SFN can be used as a diagnostic biomarker for breast cancer (Zurita et al., 2010). In the extracellular vesicles of patients with colorectal cancer, the protein level of SFN is associated with poor prognosis (Hou et al., 2022). Similarly, in serum samples of HCC patients, the level of SFN protein is higher than that in cirrhosis, chronic hepatitis, and healthy samples (Lin et al., 2017). Consequently, SFN has emerged as a serum diagnostic biomarker of HCC.

Adequate mouse models are crucial for investigating the molecular mechanisms of HCC, the function of potential oncogenes *in vivo*, and the development of new treatment strategies. Mouse HCC models include genetically engineered (Ju et al., 2016), syngeneic implantation (Bresnahan et al., 2020), humanized (Blumer et al., 2019), and chemical carcinogen-induced models (Wu et al., 2016). The allogeneic transplantation tumor model was established by subcutaneously implanting HCC cells, which offers simplicity and facilitates the easy observation of tumor progression. However, this did not represent the primary HCC

microenvironment. Genetically engineered and chemical carcinogen-induced mouse models represent primary HCC models, providing a better simulation of the liver microenvironment and a closer approximation to HCC progression. However, these models require a long process for the development of HCC. Humanized mouse models, established by *in situ* inoculation of HCC patient cells into mouse livers, better simulate the tumor microenvironment, but present technical challenges. In this study, we used genetically engineered mouse models and syngeneic implantation models to verify the role of SFN in the progression of primary and subcutaneous HCC. Future research can further investigate whether SFN directly drives HCC occurrence through SFN overexpression and knockout mouse models.

Through in-depth investigation of the molecular mechanism of SFN in regulating AKT1, our findings highlight the crucial role of two arginine sites (R56 and R129) in SFN binding, activating AKT1, and influencing HCC progression. This discovery provided a novel target for HCC treatment. In addition, our study identified that SFN binds to amino acids

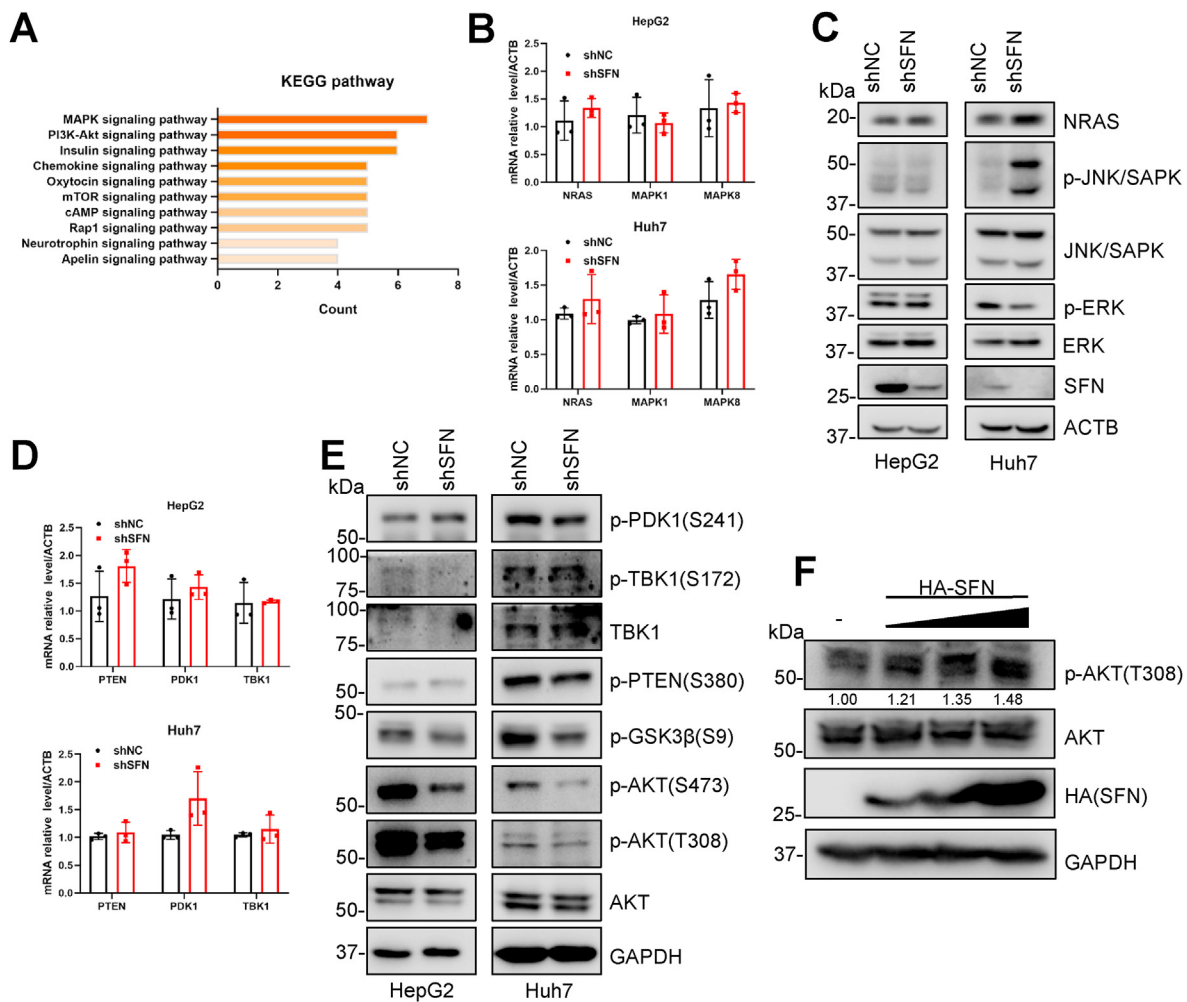


**Fig. 5. SFN supports AKT activation.**

(A) Huh7 cells were transfected with expressing Flag-tag SFN plasmid for 36 h. SFN interacting proteins in the cell lysates were immunoprecipitated with ANTI-FLAG® M2 Affinity Gel. The proteins were eluted and trypsinized to peptides. The peptides were separated by HPLC before mass spectrometry. KEGG pathway analysis for SFN interactors as display. (B) qPCR analysis of the expression levels of NRAS, MAPK1 and MAPK8 in HepG2 (top) and Huh7 (bottom) cells transduced with scrambled shRNA control (shNC) or shSFN. (C) Immunoblot analysis of the expression levels of SFN and MAPK pathway in HepG2 (left) and Huh7 (right) cells transduced with scrambled shRNA control (shNC) or shSFN. (D) qPCR analysis of the expression levels of PTEN, PDK1 and TBK1 in HepG2 (top) and Huh7 (bottom) cells transduced with scrambled shRNA control (shNC) or shSFN. (E) Immunoblot analysis of the expression levels of SFN and AKT pathway in HepG2 (left) and Huh7 (right) cells transduced with scrambled shRNA control (shNC) or shSFN. (F) Immunoblot analysis of the expression levels of SFN and AKT pathway in Huh7 cells transfected with PHA-SFN or empty vector for 36 h.

445–462 of AKT1, a sequence rich in acidic amino acids that is crucial for the interaction with SFN. Our research further confirmed that PDQDDs expression inhibits HCC progression by disrupting the interaction between SFN and AKT1. Therefore, peptide drugs designed according to the PDQDDs hold promise as a therapeutic approach for the clinical treatment of HCC with SFN overexpression.

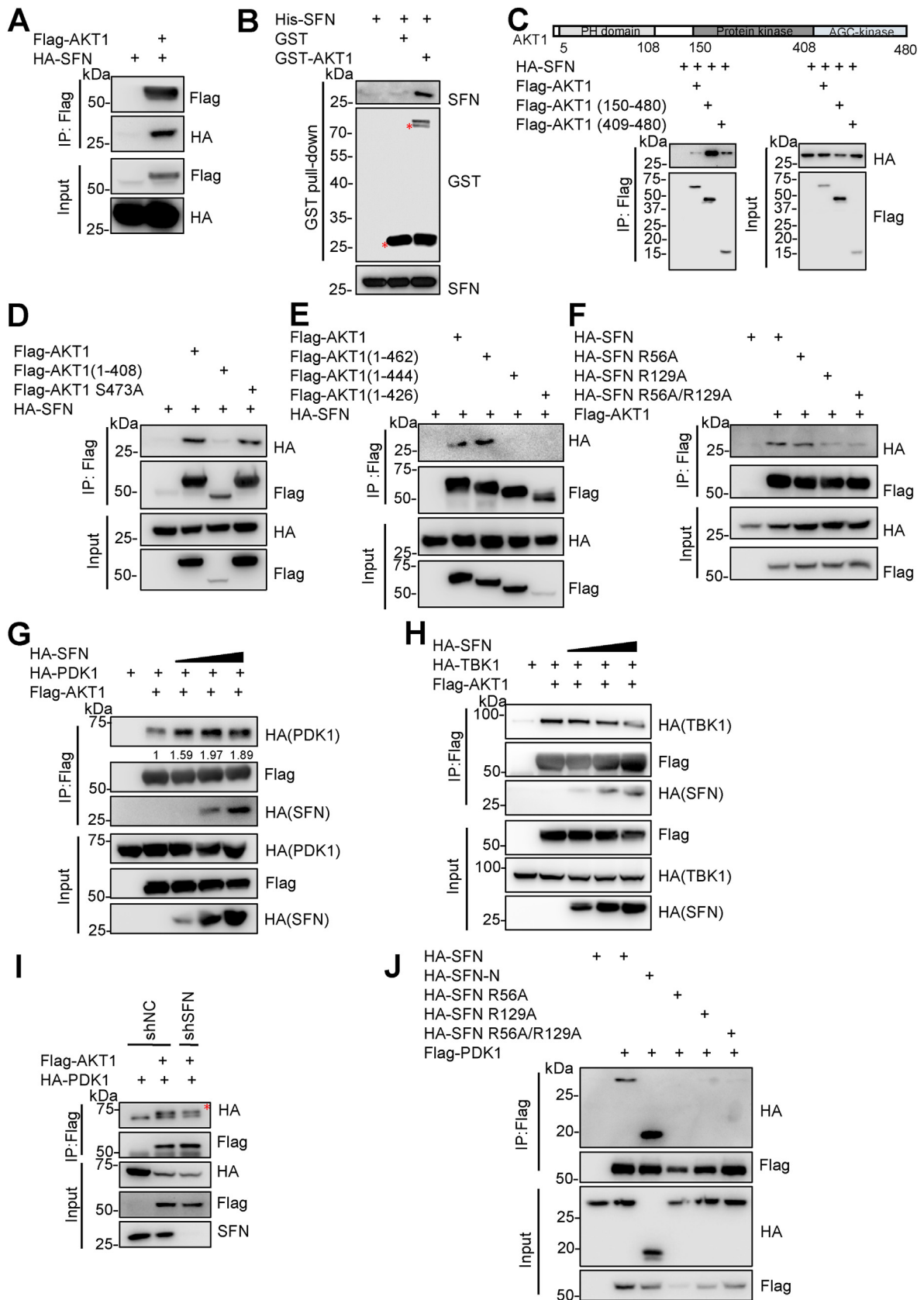
Peptide drugs have developed rapidly since the clinical application of insulin (Lau & Dunn, 2018). To date, approximately 80 peptide drugs are available on the global market (Muttenthaler et al., 2021). Peptide drugs have unique advantages in terms of clinical development and application. Their specific structure allows for a strong affinity with target proteins, enabling therapeutic effects at low doses. As their components are primarily amino acids, the toxicity and side effects of metabolites in the body are minimal. In addition, owing to mature peptide synthesis technology, the development and transformation costs of peptide drugs have been significantly reduced (Fosgerau & Hoffmann, 2015). Despite these advantages, challenges persist in the development of novel peptide drugs. Peptides are susceptible to protease degradation in the body, resulting in their low stability. However, this can be addressed through chemical modification during the synthesis process. Furthermore,

peptides exhibit poor membrane permeability, necessitating chemical modification, liposomal inclusion, or cell-penetrating peptide modification to enhance the delivery efficiency of peptide drugs (Muttenthaler et al., 2021). Based on the insights into SFN regulation of HCC and the inhibitory effect of peptides observed in our study, future investigations should focus on verifying the effects of polypeptide drugs in primary HCC models.

## 4. Materials and methods

### 4.1. Vectors and plasmids

SFN, SFN R56A, SFN R129A, SFN R56A/R129A, TBK1, and PDK1 were cloned into the pXJ40-HA vector. SFN, PDK1, AKT1, AKT1 (150–480aa), AKT1 (409–480aa), AKT1 (1–408aa), AKT1 (1–426aa), AKT1 (1–444aa), AKT1 (1–462aa), and AKT1 S473A were cloned into pXJ40-Flag. For knockdown experiments, 3' UTR SFN short hairpin RNA (shSFN) and CDS Sfn shRNA (shSfn) were constructed in pLKO.1. HA-Sfn, HA-Sfn R56A, HA-Sfn R129A, and HA-Sfn R56A/R129A were cloned into pWPI for overexpression. SFN was cloned into pAAV-CMV and pSB-GFP for



(caption on next page)

**Fig. 6. SFN promotes the interaction between PDK1 and AKT1.**

(A) HEK293T cells were co-transfected with pHA-SFN and pFlag-AKT1 or empty vector for 36 h, Flag-tag AKT1 was immunoprecipitated from HEK293T cells using anti-Flag M2 affinity gel. Immunoprecipitates were probed for Flag-tag AKT1 and HA-tag SFN. (B) Recombinant AKT1 and SFN proteins were incubated in GST pull-down binding buffer with GST-tag Purification Resin at 4 °C overnight. Glutathione-mediated affinity isolation of AKT1 (GST pull-down) was used to define the interaction between AKT1 and SFN. (C) Flag-AKT expression constructs encoding a panel of truncation variants were co-expressed with pHA-SFN in HEK293T cells for 36 h. Flag-tag AKT1 was immunoprecipitated from HEK293T cells using anti-Flag M2 affinity gel. Immunoprecipitates were probed for Flag-tag AKT1 and HA-tag SFN. (D) HEK293T cells were co-transfected with pHA-SFN and pFlag-AKT1, pFlag-AKT1 (1–408), pFlag-AKT1 S473A or empty vector for 36 h, Flag-tag AKT1 was immunoprecipitated from HEK293T cells using anti-Flag M2 affinity gel. Immunoprecipitates were probed for Flag-tag AKT1 and HA-tag SFN. (E) Flag-AKT expression constructs encoding a panel of truncation variants were co-expressed with pHA-SFN in HEK293T cells for 36 h. Flag-tag AKT1 was immunoprecipitated from HEK293T cells using anti-Flag M2 affinity gel. Immunoprecipitates were probed for Flag-tag AKT1 and HA-tag SFN. (F) HA-SFN expression constructs encoding a panel of site-directed variants were co-expressed with pFlag-AKT1 in HEK293T cells for 36 h. Immunoprecipitates were probed for Flag-tag AKT1 and HA-tag SFN. (G) HEK293T cells were co-transfected with pHA-SFN, pHA-PDK1 and pFlag-AKT1 or empty vector for 36 h, Flag-tag AKT1 was immunoprecipitated from HEK293T cells using anti-Flag M2 affinity gel. Immunoprecipitates were probed for Flag-tag AKT1, HA-tag SFN and HA-tag PDK1. (H) HEK293T cells were co-transfected with pHA-SFN, pHA-TBK1 and pFlag-AKT1 or empty vector for 36 h, Flag-tag AKT1 was immunoprecipitated from HEK293T cells using anti-Flag M2 affinity gel. Immunoprecipitates were probed for Flag-tag AKT1, HA-tag SFN and HA-tag TBK1. (I) pHA-PDK1 and pFlag-AKT1 were co-transfected into control or SFN KD Huh7 cells for 36 h, Flag-tag AKT1 was immunoprecipitated from HEK293T cells using anti-Flag M2 affinity gel. Immunoprecipitates were probed for Flag-tag AKT1 and HA-tag SFN. (J) HA-SFN expression constructs encoding a panel of site-directed variants were co-expressed with pFlag-PDK1 in HEK293T cells for 36 h. Immunoprecipitates were probed for Flag-tag PDK1 and HA-tag SFN.

overexpression experiments. PDQDDSP2A-acGFP was cloned into pWPI for the overexpression experiments. SFN was cloned into pET28a, and AKT1 was cloned into pGEX6p-1 for *in vitro* expression. pSB-cMyc-GFP, pSB100, and pX330-sgP53 were used in the hydrodynamic gene delivery-induced HCC mouse model. psPAX2 and pMD2.G were used in the lentiviral package. The pAAV2/8-RC and pHelper were used in the AAV package. The primer sequences are listed in [Table S1](#).

#### 4.2. Cell cultures and transfection

HepG2, Huh7, Li-7, Hepa1-6 and HEK293T cells were cultured in DMEM (Bio-channel, BC-M-005) supplemented with 10% FBS (LON-SERA, S711-001S), 100 U/ml penicillin and 100 µg/mL streptomycin (Gibco, 15140-122). H22 cells were cultured in RPMI 1640 (Gibco, C11875500BT) supplemented with 10% FBS (S711-001S), 100 U/ml penicillin, and 100 µg/mL streptomycin (Gibco, 15140-122). All the five cell lines were cultured at 37 °C in a 5% CO<sub>2</sub> incubator. PEI MAX 40 K (Polysciences, 24765-1) was used for the plasmid transfection.

#### 4.3. HCC patient samples

Human hepatocellular carcinoma tissues and paired adjacent normal tissues were obtained from Tongji Hospital of Huazhong University of Science and Technology. HCC specimens were obtained from a total of 21 patients (10 males and 11 females) with hepatocellular carcinoma at HCC aged 27–81 years. Ethical approval was obtained from the Ethical Committee of Tongji Hospital, Huazhong University of Science and Technology (HUST). All the patients provided written informed consent for the use of their tissue specimens. The study methodology conformed to the standards set by the Declaration of Helsinki.

#### 4.4. RNA extraction and RT-qPCR

Total RNA was extracted from cells or liver tissues using an Ultrapure RNA Kit (CWBI, CW0581M) according to the manufacturer's protocol. For cDNA synthesis, 500 ng of total RNA was reverse transcribed using ReverTra Ace qPCR RT Master Mix with gDNA Remover (TOYOBO, FSQ-301). The cDNAs were then used for real-time quantitative PCR using the FastStart Essential DNA Green Master (Roche, 06924204001). ACTB served as the internal control. The primer sequences are listed in [Table S2](#).

#### 4.5. Western blotting and Co-immunoprecipitation

Cells and tissues were lysed in RIPA buffer (Sigma, V900854) supplemented with a Protease Inhibitor Cocktail (APExBIO, K1007). 30 µg total protein samples were separated using 10% SDS-PAGE and then

transferred to a PVDF membrane. The membranes were blocked in 5% BSA and blotted with the indicated primary antibodies. β-Actin served as an internal housekeeping control.

For co-immunoprecipitation, whole-cell extracts were prepared in RIPA buffer (PUMOK, PMK0211) supplemented with a Protease Inhibitor Cocktail. FLAG-tagged proteins were immunoprecipitated using ANTI-FLAG® M2 Affinity Gel (Sigma, A2220). Flag-tagged and interacting proteins were eluted with SDS-PAGE sample buffer (50 mM Tris HCl, pH 6.8, 4% SDS, 20% (v/v) glycerol, and 0.05% bromophenol blue) and then boiled for 5 min. Antibody information is presented in [Table S3](#).

#### 4.6. Virus production and infection

For lentivirus production, pLKO.1-shRNA plasmids or pWPI-Sfn (2 µg), psPAX2(1.5 µg), and pMD2.G (0.5 µg) were co-transfected into HEK293T cells in T25 flasks. Cell supernatants were collected after 48 and 72 h and then filtered with a 0.45 µm filter member (Millipore, SLHVR33RB) to remove cell debris.

For lentivirus infection, 1 ml lentivirus supplemented with 8 µg/ml polybrene (Solarbio, H8761) was added to 6 well plate. The cell culture medium was replaced 24 h after infection. To select lenti-shRNA-infected cells, 1–10 µg/ml puromycin (P8230; Solarbio) was added to the cell culture medium. To select lenti-Sfn-infected cells, 10 µg/ml blasticidin S was added to the cell culture medium.

#### 4.7. Cell growth assay

3000 cells were plated in 96 well plate. After 0, 24, 48, and 72 h, the cell culture medium was replaced with complete medium containing 10% CCK8 (Beyotime, C0039), and the cells were incubated for 1 h. The absorbance was measured using a microtiter plate reader at 450 nm to represent cell numbers.

#### 4.8. Migration assay

Cells ( $1 \times 10^5$ ) were plated into 6.5 mm Transwell® 8.0 µm Vessels (Corning, 3422) and cultured in FBS-free medium, and medium containing 10% FBS was added to the vessels below. 24 h after plating, the cells were wiped off inside the vessels, and cells that migrated out of the vessels were fixed with 4% paraformaldehyde and stained with 0.1% crystal violet. Migrated cells were captured, and their migration ability was determined.

#### 4.9. Colony-formation assay

One thousand cells were plated in 6 well plate and cultured in complete medium for 10–14 days. The cells were fixed with 4%

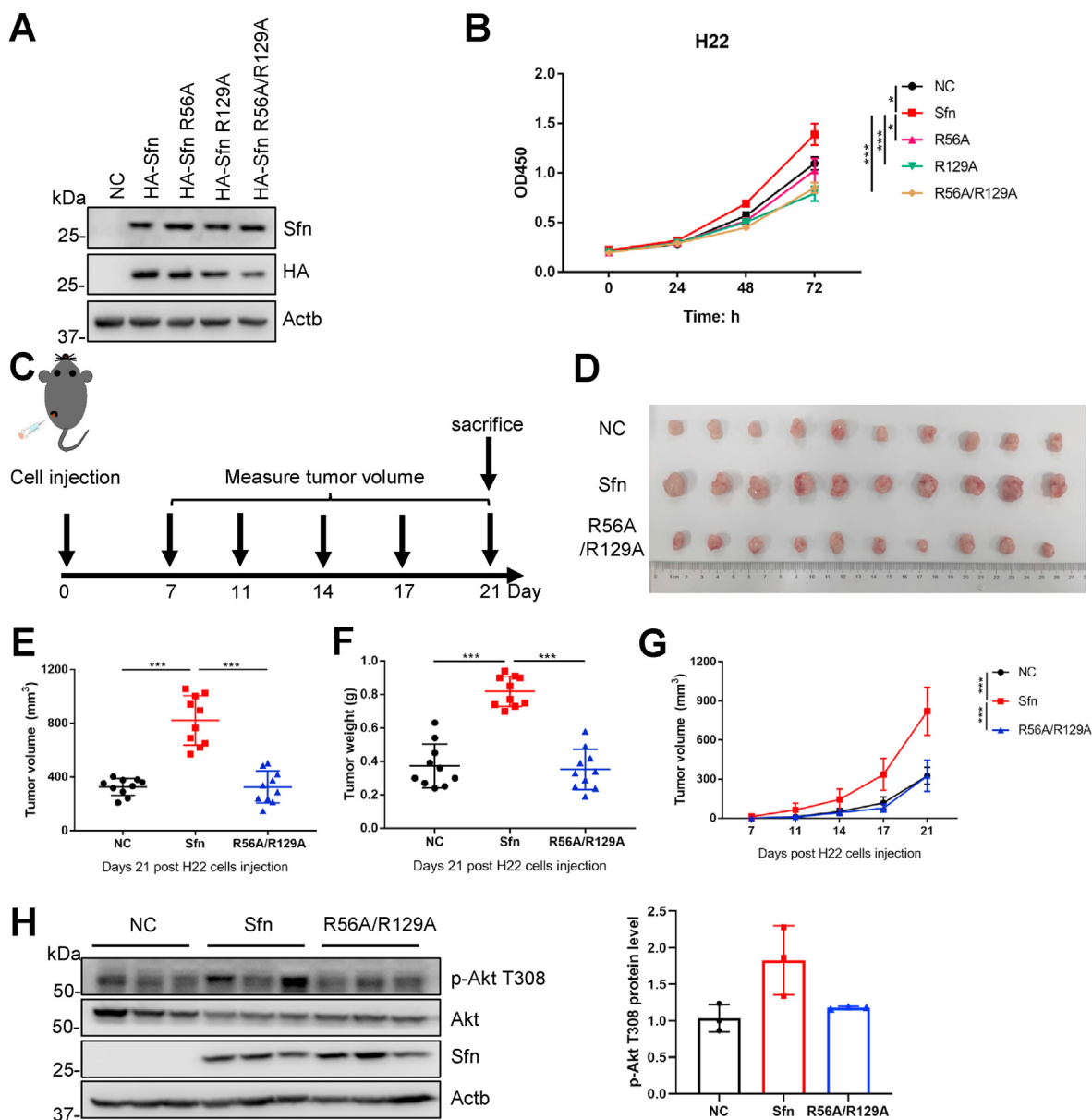


**Fig. 7. Sfn R56 and R129 are potential therapeutic targets for HCC.**

(A) H22 cells were infected with lentivirus overexpressing HA-Sfn, mutants or negative control and selected by Blasticidin. Sfn overexpression in protein level was validated by western blot with HA and Sfn antibodies. (B) Cell proliferation was measured by CCK8 in Sfn, Sfn mutants overexpression and negative control H22 cell lines. (C) Schematic for implantation assay. Mice were subcutaneously injected with  $1 \times 10^6$  Sfn, Sfn mutants overexpression and negative control H22 cells to generate a tumor model. Tumor volume was measured in 7, 11, 14, 17, 21 days post injection. Mice were sacrificed days 21 post H22 cells infection. (D) Photographs of tumors 21 days post injection of control and Sfn, Sfn mutants overexpression H22 cells implantation.  $n = 10$ . (E) Quantification of tumor volume from control and Sfn, Sfn mutants overexpression H22 cells implantation 21 days post injection.  $n = 10$ . (F) Tumor weight of control and Sfn, Sfn mutants overexpression H22 cells implantation 21 days post injection.  $n = 10$ . (G) Tumor growth curve of control and Sfn, Sfn mutants overexpression H22 cells implantation 21 days post injection.  $n = 10$ . (H) Sfn, p-Akt T308 were detected by western blot of control and Sfn, Sfn mutants overexpression H22 cells implantation (left). Statistics of p-Akt T308 level in Sfn, Sfn mutants overexpression H22 cells implantation (right).

paraformaldehyde and stained with 0.1% crystal violet. Cell numbers were calculated, and cell viability was determined.

#### 4.10. Animals

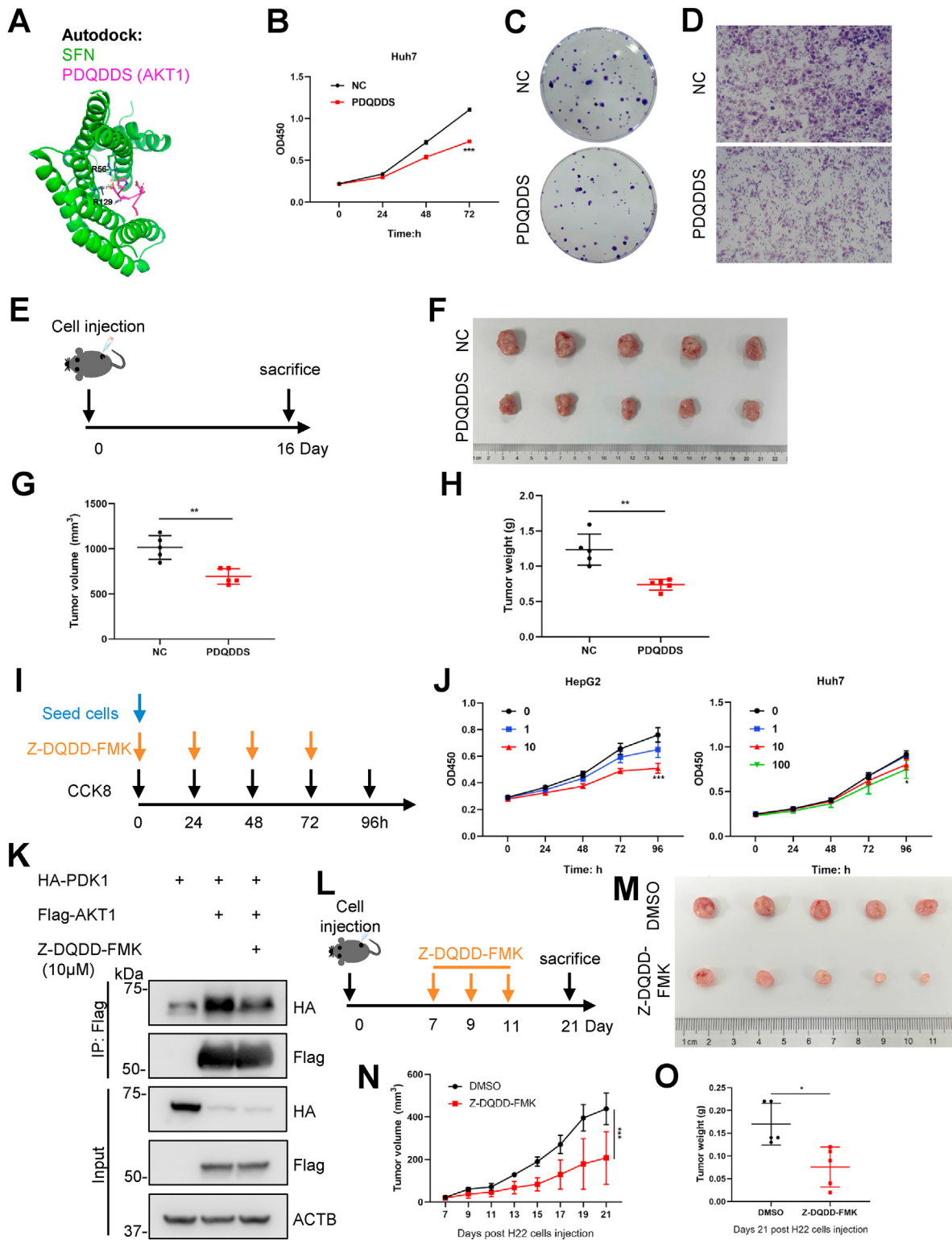
C57BL/6 male mice (6–8 weeks old) were purchased from the China Three Gorges University Laboratory Animal Center (Yichang, China). 4-week-old C57BL/6 male mice were purchased from Beijing Vital River Laboratory Animal Technology Cooperation Limited. Mice in each experiment were randomly grouped. All animal experiments were approved by the Ethics Committee of the Animal Facility of Wuhan

University.

#### 4.11. Xenograft assay

To examine Sfn knockdown cell tumor formation in C57BL/6 male mice,  $1.3 \times 10^6$  Hepa1-6 cells were resuspended in 0.1 mL PBS and injected subcutaneously into the flanks of C57BL/6 mice. The mice were sacrificed 21 days after injection, and the tumors were excised and measured.

To examine tumor formation by Sfn-overexpressing cells in C57BL/6 male mice,  $1 \times 10^6$  H22 cells were resuspended in 0.1 mL PBS and



(caption on next page)

### Fig. 8. AKT1 motif PDQDDS inhibits HCC growth by competitive binding SFN with AKT1.

(A) Molecular docking between AKT1 motif PDQDDS and SFN. (B) Huh7 cells were infected with lenti-virus expressing PDQDDS-P2A-GFP for 24 h and screened by puromycin for 72 h. Cells were plated into 96-well plate and measured for cell proliferation by CCK8. (C) Huh7 cells were infected with lenti-virus expressing PDQDDS-P2A-GFP for 24 h and screened by puromycin for 72 h. Cells were plated into 6-well plate and measured for cell proliferation by colony formation assay. (D) Huh7 cells were infected with lenti-virus expressing PDQDDS-P2A-GFP for 24 h and screened by puromycin for 72 h. Cells were plated into transwell and measured for cell migration. (E) Schematic for implantation assay. Mice were subcutaneously injected with  $1 \times 10^6$  PDQDDS-P2A-GFP overexpression and negative control H22-Sfn cells to generate a tumor model. Mice were sacrificed days 16 post H22-Sfn cells infection. (F) Photographs of tumors 16 days post injection of control and PDQDDS-P2A-GFP overexpression H22-Sfn cells implantation.  $n = 5$ . (G) Quantification of tumor volume from control and PDQDDS-P2A-GFP overexpression H22-Sfn cells implantation 16 days post injection.  $n = 5$ . (H) Tumor weight of control and PDQDDS-P2A-GFP overexpression H22-Sfn cells implantation 16 days post injection.  $n = 5$ . (I) Schematic for cell proliferation assay. (J) HepG2 (left) and Huh7 (right) cells were plated into 96-well plate, treated with Z-DQDD-FMK and measured for cell proliferation by CCK8 every 24 h. (K) pHA-PDK1 and pFlag-AKT1 or empty vector were co-transfected in Huh7 cells for 24 h and treated with  $10 \mu\text{M}$  Z-DQDD-FMK for 24 h. Flag-tag AKT1 was immunoprecipitated from Huh7 cells using anti-Flag M2 affinity gel. Immunoprecipitates were probed for Flag-tag AKT1 and HA-tag PDK1. (L) Schematic for implantation assay. Mice were subcutaneously injected with  $5 \times 10^5$  H22-Sfn cells to generate a tumor model. Tumors were treated with 5 mg/kg Z-DQDD-FMK or 1% DMSO (control group) in 7, 9, 11 days post injection. Mice were sacrificed days 21 post H22-Sfn cells infection. (M) Photographs of tumors 21 days post injection of control and Z-DQDD-FMK treated H22-Sfn cells implantation.  $n = 5$ . (N) Tumor growth curve of control and Z-DQDD-FMK treated H22-Sfn cells implantation 21 days post injection.  $n = 5$ . (O) Tumor weight of control and Z-DQDD-FMK treated H22-Sfn cells implantation 21 days post injection.  $n = 5$ .

injected subcutaneously into the flanks of C57BL/6 mice. Seven days after injection, the tumors were measured twice a week. Mice were sacrificed 21 days after injection, and the tumors were excised, weighed, and measured.

To examine the effect of Z-DQDD-FMK (Bankpeptide, MTFA30375) on H22-Sfn tumorigenic ability,  $5 \times 10^5$  H22-Sfn cells were resuspended in 0.1 mL PBS and injected subcutaneously into the flanks of C57BL/6 mice. Seven days after injection, tumors were measured every two days, and 5 mg/kg Z-DQDD-FMK or 1% DMSO (control group) in a volume of 50  $\mu\text{l}$  PBS was intratumorally administered three times every two days. Mice were sacrificed 21 days after injection, and the tumors were excised, weighed, and measured.

#### 4.12. Hydrodynamic gene delivery

C57BL/6 mice were hydrodynamically delivered with 8  $\mu\text{g}$  pSB-cMyc-GFP plasmid combined with 10  $\mu\text{g}$  pX330-sgP53 and 2  $\mu\text{g}$  pSB100 plasmids in 2 mL PBS via tail vein injections within 5 s. 37 days after injection, liver tissues were separated to determine tumor number and size.

To examine the effect of Sfn on tumorigenesis, C57BL/6 mice were hydrodynamically administered 8  $\mu\text{g}$  pSB-Sfn-GFP or blank plasmid combined with 10  $\mu\text{g}$  pX330-sgP53 and 2  $\mu\text{g}$  pSB100 plasmids in 2 mL PBS via tail vein injections within 5 s. Ten weeks after injection, liver tissues were separated to detect whether tumorigenesis was detected by H&E and Ki-67 staining.

#### 4.13. Generation and delivery of recombinant adeno-associated virus

The pAAV-CMV-Sfn or pAAV-CMV-EGFP, pAAV2/8-RC, and pHelper plasmids were co-transfected into HEK293T cells at a 1:1:1 M ratio. Eighteen hours after transfection, the cells were washed once with PBS and incubated in DMEM complete medium. Cell supernatants and cells were collected 72 h after incubation. Cells were resuspended in 1/5 supernatant and lysed by 3 times freeze-thaw cycles ( $-80 \text{ }^\circ\text{C}$ – $37 \text{ }^\circ\text{C}$ ), cell lysates were centrifuged at 3900 rpm for 15 min at  $4 \text{ }^\circ\text{C}$ . All supernatants were filtered with a 0.22  $\mu\text{m}$  filter member (Millipore, SLGPR33RB) and concentrated using a Centricon Plus-70 Centrifugal Filter (Millipore, UFC710008). AAV copy numbers were calculated using RT-qPCR.

For animal infection, 6–8-week-old C57BL/6 male mice were infected with  $1 \times 10^{11}$  copies of AAV via tail vein injections.

#### 4.14. GST pull-down

His-tagged SFN was expressed in BL21 and purified using BeyoGold™ His-tag Purification Resin (Beyotime, P2218). GST-tagged AKT1 was expressed in BL21 and purified using BeyoGold™ GST-tag Purification Resin (Beyotime, P2253). For GST pull-down, GST-tag Purification Resin were blocked by 10% goat serum, 25  $\mu\text{g}$  His-tag SFN together with 10  $\mu\text{g}$  GST-tag AKT1 or GST protein incubated in GST pull-down binding buffer

at  $4 \text{ }^\circ\text{C}$  overnight, GST-tag Purification Resin binding proteins were eluted with SDS-PAGE sample buffer and then boiled for 5 min. Direct interactions were detected using western blotting.

#### 4.15. Immunoprecipitation-mass spectrometry

The Flag-tagged SFN plasmid was transfected into Huh7 cells for 36 h. Whole-cell extracts were prepared in RIPA buffer (PUMOK, PMK0211) supplemented with a Protease Inhibitor Cocktail. FLAG-tagged proteins were immunoprecipitated using ANTI-FLAG® M2 Affinity Gel (Sigma, A2220). Flag-tagged SFN and interacting proteins were eluted with 0.2M glycine (pH 2.0) and neutralized with 1M Tris-HCl (pH 8.5). Eluted proteins were precipitated with acetone and digested overnight into peptides using trypsin (Promega, V528A). The peptides were further desalted using Pierce C18 Tips (Thermo Fisher Scientific, 87782) and used for MS analysis.

#### 4.16. Prediction of protein binding motif by AutoDock

The crystal structures of the SFN and AKT1 proteins were downloaded from the PDB protein database, and PyMOL software was used to remove excess water molecules, hydrogenate, charge, and preserve them as receptors and ligand structures for molecular docking. Molecular docking between SFN and AKT1 structures was performed using Autodock4.

#### 4.17. Correlations between candidate genes and clinical features

GEPIA (Tang et al., 2017) was used to analyze the correlations between candidate genes and overall survival in HCC. In this analysis, there were 182 HCC clinical samples with high-expression candidate genes and 182 HCC clinical samples with low-expression candidate genes. A log-rank test was performed to identify the association between candidate genes and overall survival.

#### 4.18. Ethics statement

All the patients provided written informed consent for the use of their tissue specimens. The study methodology conformed to the standards set by the Declaration of Helsinki. Ethical approval was obtained from the Ethics Committee of Tongji Hospital, Huazhong University of Science and Technology (Approval Number: TJJ-IRB20210760). All animal experiments were approved by the Ethics Committee of the Animal Facility, Wuhan University (Approval Number: WAEF-2023-0255).

#### 4.19. Statistical analysis

Data are presented as the mean  $\pm$  standard deviation (SD) ( $n \geq 3$ ). All statistical analyses were performed using the GraphPad Prism 8.0 software (GraphPad Software, USA). For clinical samples, statistical analyses

were performed using the Student's two-tailed paired *t*-test. For other samples, statistical analyses were performed using Student's two-tailed unpaired *t*-test. \*,  $P < 0.05$ , \*\*,  $P < 0.01$ , and \*\*\*,  $P < 0.001$ .

## 5. Data availability

The RNA-seq data analyzed in this study were obtained from the NCBI Gene Expression Omnibus (GEO) repository (accession numbers GSE14520 and GSE124535). The date of proteomic analysis in this study was obtained from the PRIDE database ([www.ebi.ac.uk/pride/archive](http://www.ebi.ac.uk/pride/archive), accession number PXD006512). The mass spectrometry proteomics data were deposited in the ProteomeXchange Consortium (<http://proteomecentral.proteomexchange.org>) via the iProX partner repository (Chen et al., 2022; Ma et al., 2019) with the dataset identifier PXD049217.

## Conflicts of interest

The authors disclose no conflicts.

## Declaration of competing interest

The authors declare the following financial interests/personal relationships which may be considered as potential competing interests:

Yuchen Xia reports financial support was provided by Pingyuan Laboratory. Yuchen Xia reports a relationship with National Natural Science Foundation of China that includes: funding grants. Yuchen Xia and Rong Hua have patent Z-DQDD-FMK peptide for HCC treatment pending to Wuhan KEHAO Intellectual Property. If there are other authors, they declare that they have no known competing financial interests or personal relationships that could have appeared to influence the work reported in this paper.

## CRedit authorship contribution statement

**Rong Hua:** Writing – review & editing, Writing – original draft, Methodology, Investigation. **Kaitao Zhao:** Investigation. **Zaichao Xu:** Investigation. **Yingcheng Zheng:** Investigation. **Chuanjian Wu:** Investigation. **Lu Zhang:** Investigation. **Yan Teng:** Investigation. **Jingjing Wang:** Investigation. **Mengfei Wang:** Investigation. **Jiayu Hu:** Investigation. **Lang Chen:** Investigation. **Detian Yuan:** Resources, Methodology. **Wei Dong:** Resources, Methodology. **Xiaoming Cheng:** Supervision, Resources. **Yuchen Xia:** Writing – review & editing, Resources, Project administration, Funding acquisition, Conceptualization.

## Acknowledgments

This work was supported by the National Key Research and Development Program of China (No. 2023YFC2308500), the Open Grant from the Pingyuan Laboratory (2023PY-OP-0101), the Fundamental Research Funds for the Central Universities (project no. 2042024kf0026, 2042022kf1215, 2042023kf0129, and 2042021gf0013), the National Natural Science Foundation of China (project nos. 81971936, 32100125, and 32300131), Hubei Province's Outstanding Medical Academic Leader Program, and Basic and Clinical Medical Research Joint Fund of Zhongnan Hospital, Wuhan University. We thank the staff of the Research Center for Medicine and Structural Biology of Wuhan University for their technical assistance.

## Appendix A. Supplementary data

Supplementary data to this article can be found online at <https://doi.org/10.1016/j.cellin.2024.100178>.

## References

- Arakawa, N., Ushiki, A., Abe, M., Matsuyama, S., Saito, Y., Kashiwada, T., Horimasu, Y., Gemma, A., Tatsumi, K., Hattori, N., et al. (2022). Stratifin as a novel diagnostic biomarker in serum for diffuse alveolar damage. *Nature Communications*, 13, 5854.
- Blumer, T., Fofana, I., Matter, M. S., Wang, X., Montazeri, H., Calabrese, D., Coto-Llerena, M., Boldanova, T., Nuciforo, S., Kancherla, V., et al. (2019). Hepatocellular carcinoma xenografts established from needle biopsies preserve the characteristics of the originating tumors. *Hepatology communications*, 3, 971–986.
- Bresnahan, E., Lindblad, K. E., Ruiz de Galarreta, M., & Lujambio, A. (2020). Mouse models of oncoimmunology in hepatocellular carcinoma. *Clinical Cancer Research: An Official Journal of the American Association for Cancer Research*, 26, 5276–5286.
- Chen, T., Ma, J., Liu, Y., Chen, Z., Xiao, N., Lu, Y., Fu, Y., Yang, C., Li, M., Wu, S., et al. (2022). iProX in 2021: connecting proteomics data sharing with big data. *Nucleic Acids Research*, 50, D1522–d1527.
- Chen, Y., Ruggeri, Z. M., & Du, X. (2018). 14-3-3 proteins in platelet biology and glycoprotein Ib-IX signaling. *Blood*, 131, 2436–2448.
- Cooper, J. M., Ou, Y. H., McMillan, E. A., Vaden, R. M., Zaman, A., Bodemann, B. O., Makkar, G., Posner, B. A., & White, M. A. (2017). TBK1 provides context-selective support of the activated AKT/mTOR pathway in lung cancer. *Cancer Research*, 77, 5077–5094.
- Forner, A., Llovet, J. M., & Bruix, J. (2012). Hepatocellular carcinoma. *Lancet (London, England)*, 379, 1245–1255.
- Forner, A., Reig, M., & Bruix, J. (2018). Hepatocellular carcinoma. *Lancet (London, England)*, 391, 1301–1314.
- Fosgerau, K., & Hoffmann, T. (2015). Peptide therapeutics: Current status and future directions. *Drug Discovery Today*, 20, 122–128.
- Hermeking, H., Lengauer, C., Polyak, K., He, T. C., Zhang, L., Thiagalingam, S., Kinzler, K. W., & Vogelstein, B. (1997). 14-3-3sigma is a p53-regulated inhibitor of G2/M progression. *Molecular Cell*, 1, 3–11.
- Hou, W., Pan, M., Xiao, Y., & Ge, W. (2022). Serum extracellular vesicle stratifin is a biomarker of perineural invasion in patients with colorectal cancer and predicts worse prognosis. *Frontiers Oncology*, 12, Article 912584.
- Hoxhaj, G., & Manning, B. D. (2020). The PI3K-AKT network at the interface of oncogenic signalling and cancer metabolism. *Nature Reviews Cancer*, 20, 74–88.
- Jiang, Y., Sun, A., Zhao, Y., Ying, W., Sun, H., Yang, X., Xing, B., Sun, W., Ren, L., Hu, B., et al. (2019). Proteomics identifies new therapeutic targets of early-stage hepatocellular carcinoma. *Nature*, 567, 257–261.
- Jiang, Q., Zhang, X., Dai, X., Han, S., Wu, X., Wang, L., Wei, W., Zhang, N., Xie, W., & Guo, J. (2022). S6K1-mediated phosphorylation of PDK1 impairs AKT kinase activity and oncogenic functions. *Nature Communications*, 13, 1548.
- Ju, H. L., Han, K. H., Lee, J. D., & Ro, S. W. (2016). Transgenic mouse models generated by hydrodynamic transfection for genetic studies of liver cancer and preclinical testing of anti-cancer therapy. *International Journal of Cancer*, 138, 1601–1608.
- Kaplan, A., Bueno, M., & Fournier, A. E. (2017). Extracellular functions of 14-3-3 adaptor proteins. *Cellular Signalling*, 31, 26–30.
- Kim, J. Y., Kim, M. J., Lee, J. S., Son, J., Kim, D. H., Lee, J. S., Jeong, S. K., Chun, E., & Lee, K. Y. (2022). Stratifin (SFN) regulates lung cancer progression via nucleating the Vps34-BECN1-TRAF6 complex for autophagy induction. *Clinical and Translational Medicine*, 12, e896.
- Kim, Y., Shiba-Ishii, A., Nakagawa, T., Iemura, S. I., Natsume, T., Nakano, N., Matsuoka, R., Sakashita, S., Lee, S., Kawaguchi, A., et al. (2018). Stratifin regulates stabilization of receptor tyrosine kinases via interaction with ubiquitin-specific protease 8 in lung adenocarcinoma. *Oncogene*, 37, 5387–5402.
- Kudo, M., Finn, R. S., Qin, S., Han, K. H., Ikeda, K., Piscaglia, F., Baron, A., Park, J. W., Han, G., Jasse, J., et al. (2018). Lenvatinib versus sorafenib in first-line treatment of patients with unresectable hepatocellular carcinoma: A randomised phase 3 non-inferiority trial. *Lancet (London, England)*, 391, 1163–1173.
- Lau, J. L., & Dunn, M. K. (2018). Therapeutic peptides: Historical perspectives, current development trends, and future directions. *Bioorganic & Medicinal Chemistry*, 26, 2700–2707.
- Lencioni, R., Kudo, M., Ye, S. L., Bronowicki, J. P., Chen, X. P., Dagher, L., Furuse, J., Geschwind, J. F., de Guevara, L. L., Papandreou, C., et al. (2014). GIDEON (global investigation of therapeutic DEcision) in hepatocellular carcinoma and of its treatment with sorafenib: Second interim analysis. *International Journal of Clinical Practice*, 68, 609–617.
- Lin, H., Jiao, X., Yu, B., Du, J., Xu, H., Dong, A., & Wan, C. (2017). Clinical significance of serum 14-3-3 beta in patients with hepatocellular carcinoma. *Cancer Biomarkers: Section A of Disease Markers*, 20, 143–150.
- Liu, R., Li, H. F., & Li, S. (2024). PD-1-mediated inhibition of T cell activation: Mechanisms and strategies for cancer combination immunotherapy. *Cell insight*, 3, Article 100146.
- Liu, Q., Li, J., Zhang, W., Xiao, C., Zhang, S., Nian, C., Li, J., Su, D., Chen, L., Zhao, Q., et al. (2021). Glycogen accumulation and phase separation drives liver tumor initiation. *Cell*, 184, 5559–5576.e5519.
- Llovet, J. M., Castet, F., Heikenwalder, M., Maini, M. K., Mazzaferro, V., Pinato, D. J., Pikarsky, E., Zhu, A. X., & Finn, R. S. (2022). Immunotherapies for hepatocellular carcinoma. *Nature Reviews Clinical Oncology*, 19, 151–172.
- Llovet, J. M., Kelley, R. K., Villanueva, A., Singal, A. G., Pikarsky, E., Roayaie, S., Lencioni, R., Koike, K., Zucman-Rossi, J., & Finn, R. S. (2021). Hepatocellular carcinoma. *Nature Reviews Disease Primers*, 7, 6.

- Llovet, J. M., Real, M. I., Montaña, X., Planas, R., Coll, S., Aponte, J., Ayuso, C., Sala, M., Muchart, J., Solà, R., et al. (2002). Arterial embolisation or chemoembolisation versus symptomatic treatment in patients with unresectable hepatocellular carcinoma: A randomised controlled trial. *Lancet (London, England)*, *359*, 1734–1739.
- Ma, J., Chen, T., Wu, S., Yang, C., Bai, M., Shu, K., Li, K., Zhang, G., Jin, Z., He, F., et al. (2019). iProX: an integrated proteome resource. *Nucleic Acids Research*, *47*, D1211–d1217.
- Marasco, G., Colecchia, A., Colli, A., Ravaoli, F., Casazza, G., Bacchi Reggiani, M. L., Cucchetti, A., Cescon, M., & Festi, D. (2019). Role of liver and spleen stiffness in predicting the recurrence of hepatocellular carcinoma after resection. *Journal of Hepatology*, *70*, 440–448.
- Mayer, I. A., & Arteaga, C. L. (2016). The PI3K/AKT pathway as a target for cancer treatment. *Annual Review of Medicine*, *67*, 11–28.
- Muttenthaler, M., King, G. F., Adams, D. J., & Alewood, P. F. (2021). Trends in peptide drug discovery. *Nature Reviews Drug Discovery*, *20*, 309–325.
- Na, T. Y., Schecterson, L., Mendonsa, A. M., & Gumbiner, B. M. (2020). The functional activity of E-cadherin controls tumor cell metastasis at multiple steps. *Proceedings of the National Academy of Sciences of the United States of America*, *117*, 5931–5937.
- Neuzillet, C., Tijeras-Raballand, A., de Mestier, L., Cros, J., Faivre, S., & Raymond, E. (2014). MEK in cancer and cancer therapy. *Pharmacology & Therapeutics*, *141*, 160–171.
- Pair, F. S., & Yacoubian, T. A. (2021). 14-3-3 proteins: Novel pharmacological targets in neurodegenerative diseases. *Trends in Pharmacological Sciences*, *42*, 226–238.
- Pellegrino, R., Calvisi, D. F., Neumann, O., Kolluru, V., Wesely, J., Chen, X., Wang, C., Wuestefeld, T., Ladu, S., Elgohary, N., et al. (2014). EEF1A2 inactivates p53 by way of PI3K/AKT/mTOR-dependent stabilization of MDM4 in hepatocellular carcinoma. *Hepatology*, *59*, 1886–1899.
- Plummer, M., de Martel, C., Vignat, J., Ferlay, J., Bray, F., & Franceschi, S. (2016). Global burden of cancers attributable to infections in 2012: A synthetic analysis. *Lancet Global Health*, *4*, e609–e616.
- Roessler, S., Jia, H. L., Budhu, A., Forgues, M., Ye, Q. H., Lee, J. S., Thorgeirsson, S. S., Sun, Z., Tang, Z. Y., Qin, L. X., et al. (2010). A unique metastasis gene signature enables prediction of tumor relapse in early-stage hepatocellular carcinoma patients. *Cancer Research*, *70*, 10202–10212.
- Sapisochin, G., & Bruix, J. (2017). Liver transplantation for hepatocellular carcinoma: Outcomes and novel surgical approaches. *Nature Reviews Gastroenterology & Hepatology*, *14*, 203–217.
- Schulze, K., Nault, J. C., & Villanueva, A. (2016). Genetic profiling of hepatocellular carcinoma using next-generation sequencing. *Journal of Hepatology*, 1031–1042.
- Shiba-Ishii, A., Hong, J., Hirokawa, T., Kim, Y., Nakagawa, T., Sakashita, S., Sakamoto, N., Kozuma, Y., Sato, Y., & Noguchi, M. (2019). Stratifin inhibits SCF(FBW7) formation and blocks ubiquitination of oncoproteins during the course of lung adenocarcinogenesis. *Clinical Cancer Research: An Official Journal of the American Association for Cancer Research*, *25*, 2809–2820.
- Sung, H., Ferlay, J., Siegel, R. L., Laversanne, M., Soerjomataram, I., Jemal, A., & Bray, F. (2021). Global cancer statistics 2020: GLOBOCAN estimates of incidence and mortality worldwide for 36 cancers in 185 countries. *Ca - a Cancer Journal for Clinicians*, *71*, 209–249.
- Tang, Z., Li, C., Kang, B., Gao, G., Li, C., & Zhang, Z. (2017). Gepia: A web server for cancer and normal gene expression profiling and interactive analyses. *Nucleic Acids Research*, *45*, W98–w102.
- Tang, M., Zhao, Y., Zhao, J., Wei, S., Liu, M., Zheng, N., Geng, D., Han, S., Zhang, Y., Zhong, G., et al. (2022). Liver cancer heterogeneity modeled by in situ genome editing of hepatocytes. *Science Advances*, *8*, Article eabn5683.
- Vogel, A., Meyer, T., Sapisochin, G., Salem, R., & Saborowski, A. (2022). Hepatocellular carcinoma. *Lancet (London, England)*, *400*, 1345–1362.
- Wu, F. Q., Fang, T., Yu, L. X., Lv, G. S., Lv, H. W., Liang, D., Li, T., Wang, C. Z., Tan, Y. X., Ding, J., et al. (2016). ADRB2 signaling promotes HCC progression and sorafenib resistance by inhibiting autophagic degradation of HIF1 $\alpha$ . *Journal of Hepatology*, *65*, 314–324.
- Yang, H. Y., Wen, Y. Y., Chen, C. H., Lozano, G., & Lee, M. H. (2003). 14-3-3 sigma positively regulates p53 and suppresses tumor growth. *Molecular and Cellular Biology*, *23*, 7096–7107.
- Yang, L., Zhang, Z., Sun, Y., Pang, S., Yao, Q., Lin, P., Cheng, J., Li, J., Ding, G., Hui, L., et al. (2020). Integrative analysis reveals novel driver genes and molecular subclasses of hepatocellular carcinoma. *Aging*, *12*, 23849–23871.
- Zhao, K., Liu, A., & Xia, Y. (2020). Insights into hepatitis B virus DNA integration-55 Years after virus discovery. *Innovation*, *1*, Article 100034.
- Zhao, X., Wang, E., Xu, H., & Zhang, L. (2023). Stratifin promotes the growth and proliferation of hepatocellular carcinoma. *Tissue and Cell*, *82*, Article 102080.
- Zurita, M., Lara, P. C., del Moral, R., Torres, B., Linares-Fernández, J. L., Arrabal, S. R., Martínez-Galán, J., Oliver, F. J., & Ruiz de Almodóvar, J. M. (2010). Hypermethylated 14-3-3-sigma and ESR1 gene promoters in serum as candidate biomarkers for the diagnosis and treatment efficacy of breast cancer metastasis. *BMC Cancer*, *10*, 217.